Atomically-Resolved Characterization of Optically-Driven Ligand Reconfiguration on Nanoparticle Catalyst Surfaces

Mary O. Olagunju,[1] Yang Liu,[2] Anatoly I. Frenkel,[2,3,] Marc R. Knecht, [1,4,]**

1. Department of Chemistry, University of Miami, 1301 Memorial Drive, Coral Gables, Florida 33146, United States

2. Department of Materials Science and Chemical Engineering, Stony Brook University, Stony Brook, New York 11794, USA.

3. Chemistry Division, Brookhaven National Laboratory, Upton, New York 11973, USA.

4. Dr. J.T. Macdonald Foundation Biomedical Nanotechnology Institute, university of Miami, UM Life Science Technology Building, 1951 NW 7th Ave, Suite 475, Miami, Florida 33136, USA.

To whom correspondence should be address: MRK – knecht@miami.edu; AIF - anatoly.frenkel@stonybrook.edu

ABSTRACT

Dynamic ligand layers on nanoparticle surfaces could prove to be critically important to enhance the functionality of individual materials. Such capabilities could complement the properties of the inorganic component to provide multifunctionality or the ability to be remotely actuated. Peptide-based ligands have demonstrated the ability to be remotely responsive to structural changes when adsorbed to nanoparticle surfaces via incorporation of photoswitches into their molecular structure. In this contribution, direct spectroscopic evidence of the remote actuation of a photoswitchable peptide adsorbed onto Au nanoparticles is demonstrated using X-ray Absorption Fine Structure spectroscopic methods. Characterization before and after photoswitching confirmed changes in the surface ligand conformation, which was correlated directly to variations in the catalytic application of the materials for nitrophenol reduction processes. In addition, the catalytic application of the materials was demonstrated to be significantly sensitive to the structure of the nitrophenol substrate used in the reaction, suggesting that changes in the reactivity are likely based upon the peptide conformation and substrate structure. Such results confirm that surface ligands can be remotely reconfigured on nanoparticle surfaces, providing pathways to apply such capabilities to a variety of applications beyond catalysis ranging from drug delivery to sensing.

INTRODUCTION

The realization of dynamic, functional nanoparticle (NP) interfaces that structurally reconfigure using external stimulus represents a grand challenge in nanomaterials.[1, 2] In this regard, these materials are designed to present the surface bound ligands in an initial configuration, which, upon exposure to a specific trigger, undergo a structural transformation to a second conformation.[3, 4] A second stimulus can then be used to return the ligands to the initial configuration with negligible structural changes to the inorganic component.[5] Such materials could make immediate impacts for applications in targeted drug delivery, biosensing, information storage, catalysis, etc.[6-8] Unfortunately, the ability to remotely and reversibly actuate structural changes of ligands bound to a NP surface is highly challenging.[7] The ligands need to be designed to possess both significant affinity for the target inorganic material and a moiety that is responsive to the external stimulus to drive the structural change.[9, 10] In addition, the external stimulus needs to also be of sufficiently low enough energy such that it does not adversely affect or degrade the material.[5] For instance, optical irradiation with light may be an ideal stimulus over heat that could lead to particle degradation and bulk precipitation.[11, 12] Taking all of these ligand/NP structural considerations into account, as well as the external stimulus factors for responsive structural changes, raises the complexity of these responsive material systems.

Bio-inspired, peptide-based approaches have recently been demonstrated with the ability to reversibly reconfigure the biomolecules when bound to NP surfaces using light as the external stimulus.[13, 14] For this, peptides with affinity for noble metal NPs were used with an azobenzene photoswitch chemically integrated into the sequence that can isomerize between the *trans* and *cis* conformation upon light irradiation. For this process, the AuBP1 peptide (WAGAKRLVLRRE) has been employed, which was originally identified with affinity for Au.[11] The photoswitch was

subsequently incorporated via thiol-maleimide coupling.[3] To this end, the azobenzene was synthesized with two flanking maleimide groups (termed MAM), which can be coupled into a cysteine thiol moiety synthetically added to the peptide. This allows for a bio-orthogonal coupling process to incorporate the photoswitch at precise locations within the biomolecule. Once synthesized, these conjugated peptides are used to prepare Au NPs by binding to the metallic surface, stabilizing the colloidal material suspension.[14] Initially, the peptides are bound to the NPs in the *trans* configuration, where switching to the *cis* conformation is achieved using UV light, thus reconfiguring the bio-overlayer structure. Irradiating the sample with visible light triggers the azobenzene to switch back to the *trans* conformation, restoring the original morphology of the peptides on the NP surface. Such switching between the *trans* and *cis* conformation can be processed for numerous cycles with negligible impacts on the overall NP structure.[14]

With the ability to change the bioligand overlayer structure between two different conformations, changes in the NP catalytic reactivity have been observed.[5, 14] To this end, when Au NPs capped the AuBP1 peptide with the photoswitch incorporated at the C-terminus (termed AuBP1C-MAM) was used to drive catalytic reduction of 4-nitrophenol in water, the reaction was notably faster with the peptides in the *trans* conformation over the *cis*.[14] This difference in reactivity was the result of a higher activation energy for the NPs in the *cis* conformation as compared to the *trans*. Such changes in reactivity between the *cis* and *trans* conformation of the biomolecule is sensitive to the peptide sequence, photoswitch position, and underlying metallic composition.[5, 13-15] While catalytic differences have been observed, direct, spectroscopic conformation of the bioligand structural changes remains elusive. Such information is important to confirm that changes in the peptide orientation are indeed occurring, which is anticipated to alter the amount or type of reactive catalytic surface area available to drive the reaction. By having

a higher amount of available reactive surface area or type of active sites exposed, changes in the catalytic rates are also likely based upon the ligand employed. Unfortunately, no significant understanding of how the reactant structure affects the overall catalytic process has been considered, which could be important to probe the overall degree of reactivity differences between the peptides in the two different conformations.

In this contribution, we present direct evidence supporting photo-driven peptide structural conformation changes on Au NP surfaces by correlative studies using surface-sensitive spectroscopy and probe reaction. For these studies, the AuBP1 peptide was used with photoswitch incorporation at either the N- or C-terminus (termed MAM-CAuBP1 and AuBP1C-MAM, respectively). The NP structural conformations were probed using X-ray Absorption Fine Structure (XAFS) spectroscopy-based methods with the peptides in both the *trans* and *cis* conformations. To complement spectroscopic studies, the effect of catalyst structure was examined for nitrophenol-based reduction. The combined results confirmed that photoswitching of the peptide conformation does occur on the NPs, supporting prior computational results;[3] however, they also suggest that the degree of structural change may be affected by the position of the azobenzene within the peptide sequence (N- versus C-terminus). Previous studies have only examined a single substrate (4-nitrophenol) for reactivity.[14, 15] This work revealed that changes in the nitro group position, as well as the number of nitro groups may greatly affect the overall NP reactivity based upon the peptide conformation. These results demonstrated catalytic sensitivity to the overall reactant structure, in combination with the peptide sequence and photoswitch conformation. Such results are important for the design of surface reconfigurable ligands for NPs to allow for selective property control.

MATERIALS AND METHODS

Materials

Hydrogen tetrachloroaurate (III) trihydrate ($HAuCl_4 \cdot 3H_2O$, 99.9%) and 4-nitrophenol were purchased from Alfa-Aesar. Sodium borohydride ($NaBH_4$), 2,3-dinitropenol, 2,4-dinitrophenol, and 3,4-dinitrophenol were obtained from Sigma-Aldrich. 2-Nitrophenol and 3-nitrophenol were purchased from Acros Organics. All peptide sequences were purchased from Genscript at 95% purity. *N,N*-dimethylformamide (DMF) was purchased from Millipore. Finally, all chemicals were used as received and ultrapure water (18.2 MΩ.cm) was used for all experiments.

Methods

Coupling of the Photoswitch. Coupling of the MAM to the peptide was carried out through standard thiol–maleimide coupling protocols.[16] Excess MAM was used during the reaction to ensure only a single peptide was coupled with the photoswitch. Once the coupling was complete, the reaction product was purified using the reverse phase HPLC (Waters Co. Delta 600 with 2498 UV–vis detector) and the coupled biomolecule was confirmed using MALDI-TOF mass spectrometry (Bruker Autoflex speed LRF).

Peptide-Capped NP Synthesis. NP synthesis followed previously published procedures.[14] In a glass vial, 2.0 mL of 0.25 mM MAM-containing peptide was diluted with 2.99 mL water, followed by the addition of 10 μL of 0.10 M $HAuCl_4$. The solution was stirred at room temperature for 15 min to enable the metal ions to complex with the peptide. Afterwards, 30 μL of cold 0.10 M $NaBH_4$ was slowly added. The mixture was swirled twice and then left to react on the benchtop for 24 h undisturbed.

Characterization

The optical properties of the peptide-capped NPs were probed using an Agilent 8453 UV–vis spectrophotometer with a 1 cm path length quartz cuvette. The size and morphology of the materials were examined using a Tecnai F30 TEM produced by FEI operating at 300 kV. TEM samples were prepared by drop-casting 10 μL of the NPs onto a carbon-coated Cu TEM grid. For sizing, at least 100 individual NPs from the TEM images were measured.

XAFS spectroscopy was used to provide local structural information of the Au NPs with different peptides in both conformations. The solution samples were sealed in the cylindrical Kapton sample holder (~5mm ID) and measured at the ISS beamline (8-ID) at the National Synchrotron Light Source-II (NSLS-II) at Brookhaven National Laboratory at the Au-L_3 edge. For each sample, at least 50 scans were collected. After the initial measurement, the samples with the peptides in the *trans* configuration were exposed to UV light from a hand help UV lamp for 30 min to switch the biomolecules to the *cis* conformation. These samples were then measured by XAFS again and the spectral changes caused by the changes in the ligand overlayer structure were analyzed. A specially designed sample with a peptide on the surface but without a photoswitch (and thus not expected to be sensitive to the light exposure) was also measured as a control sample, to obtain the baseline sensitivity information of XAFS to the catalyst restructuring in the two other light-sensitive samples. Au foil was measured in the same experiments in reference mode for energy calibration and alignment.

Catalytic Reaction Analysis

To test the catalytic reactivity of the NPs, the reduction of nitrophenol-based substrates was carried out using previously described methods.[14, 17] In a 1 cm path length cuvette, 1.1 mL of ultra-pure

water was mixed with 250 μL of the NP solution and 50 μL of the desired nitrophenol compound (2.0 mM in water) for 5 min. Afterwards, 100 μL of $NaBH_4$ (0.5 M) was added, initiating the reaction, which was monitored using UV-vis spectrophotometry. The same reaction process was conducted for each NP in both the *cis* and *trans* conformations. For reactions in the *cis* conformation, the NPs were photoswitched for 30 min to reach the photostationary state prior to catalytic studies.

RESULTS AND DISCUSSION

The photoswitchable peptides were produced by incorporating the MAM moiety into a free thiol group in the peptide sequence. To integrate the MAM unit to the biomolecule, a cysteine residue was added either at the N- or C- terminus of the parent AuBP1 peptide. The reaction was processed in DMF, from which the bioconjugated sequence was purified via HPLC and confirmed with MALDI-TOF mass spectrometry. Such methods are identical to those previously used for this reaction process.[3]

Synthesis, Characterization, and Biointerface Reconfiguration via Photoswitching

Peptide-capped Au NPs were synthesized using either the MAM-CAuBP1 or AuBP1C-MAM molecules in water via standard methods (Scheme 1).[14, 18] In general, Au^{3+} ions were complexed with the selected peptide at a Au^{3+}:peptide ratio of 2:1. After 15 min, the system was reduced with $NaBH_4$ to generate

Scheme 1. Peptide-based Au NP synthesis and bio-overlayer optical reconfiguration via photoswitch (MAM) activation.

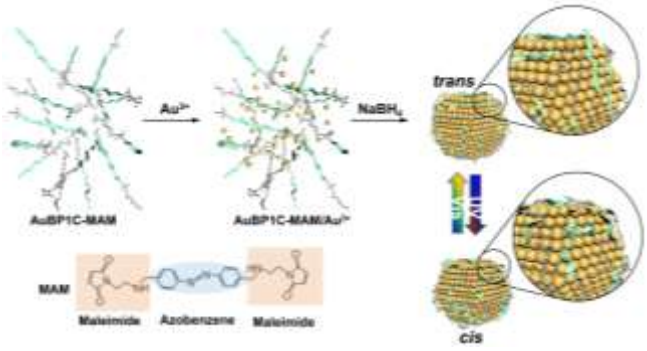

the colloidal NP suspension. This process generated a wine red solution color that was generally stable with no evidence of bulk material precipitation. The materials were allowed to reduce for 24 h prior to further studies (*e.g.* characterization or catalysis).

Initial NP characterization focused on UV-vis spectroscopy of the material synthesis process (Figures 1 a and b). As shown in Figure 1a for the AuBP1C-MAM system, the black spectrum arises from the peptide only with two absorbances centered at 330 and 450 nm. Both of these peaks are attributed to the transitions of the azobenzene photoswitch (π-π* at 330 nm and n-π* at 450 nm), providing an optical handle on the isomerization process (*vida infra*).[3] After complexation with Au^{3+} ions (red plot), negligible changes in the sample spectrum were observed, as anticipated. Upon reduction of Au^{3+} ions with $NaBH_4$ (blue plot), a significant increase in absorbance towards lower wavelengths was noted, which is consistent with NP production.[19] Similar results were observed with the MAM-CAuBP1 Au NPs (Figure 1b), suggesting that the position of the MAM unit did not inhibit NP production and stabilization. In both systems, the π-π* transition of azobenzene remains in the sample; however, the weaker n-π* absorption is not observed due to the inherent absorptivity of the NPs at this region.

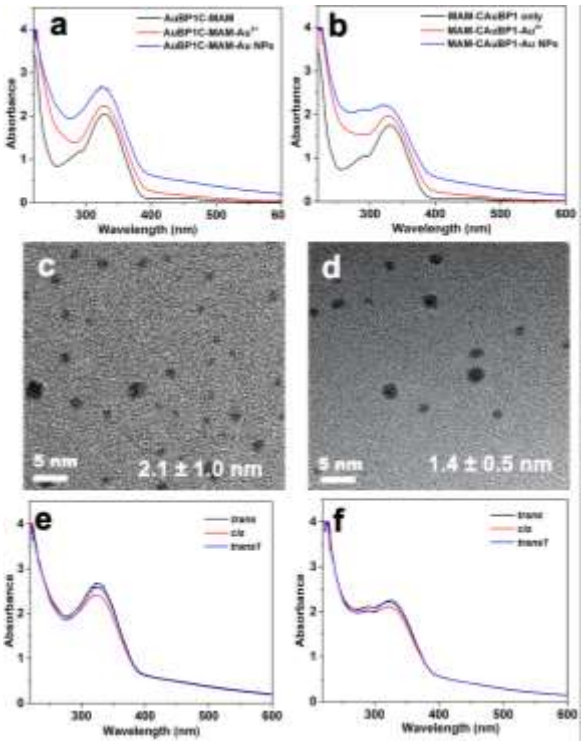

Figure 1. Characterization of NP synthesis using the photoswitchable peptides. Parts (a and b) present the UV-vis analysis, while parts (c and d) show TEM images of the prepared NPs. Parts (e and f) display the UV-vis results for photoswitching reversibility for the peptides containing the MAM unit. Analysis using the AuBP1C-MAM peptide is presented in parts (a, c, and e), while the NPs using the MAM-CAuBP1 are shown in parts (b, d, and f).

While the UV-vis studies were suggestive of NP formation, TEM imaging of the sample was used to confirm material production and measure particle sizes. Figure 1c displays a TEM image of the AuBP1C-MAM-capped Au NPs. From this analysis, it was evident that spherically shaped materials were prepared using the peptide. Sizing of at least 100 individual NPs over multiple locations on the grid surface indicated that the sample possessed an average diameter of 2.1 ± 1.0 nm. Similar results were achieved from the Au NPs capped with the MAM-CAuBP1 peptide (Figure 1c). For these materials, spherical Au NPs were again observed with an average size of 1.4 ± 0.5 nm. Such results are generally consistent with previous studies.[14]

Upon confirmation of the structure of the materials, the photoswitching ability of the MAM moiety was probed using UV-vis spectroscopy (Figure 1e-f). For both NP systems, the peptide was initially in the *trans* conformation. To switch from *trans* to *cis*, the NPs were illuminated using a handheld UV light (λ = ~365 nm) for 30 min. To restore the initial configuration, the NPs were irradiated under white light (λ = ~440 nm) for 30 min. In both cases, the photostationary state was achieved. Figure 1e presents the photoswitching of AuBP1C-MAM-capped Au NPs focusing on the π – π* transition at 330 nm. This band is highly sensitive to the azobenzene isomerization state and decreases in intensity for *trans* to *cis* switching, while it will increase in intensity for *cis* to *trans* switching. For these NPs before irradiation (black spectrum), the 330 nm peak decreased in intensity after UV irradiation (red spectrum), consistent with *trans* to *cis* switching of the MAM moiety. Subsequently, the system was irradiated with white light, inducing *cis* to *trans* switching, resulting in a near restoration of the π – π* transition (blue spectrum). During this process no change in the UV-vis spectrum at regions outside the 330 nm peak were evident and no material precipitation were observed, consistent the NPs remaining stable in solution. Identical results were observed for the MAM-CAuBP1 capped Au NPs (Figure 1f), confirming peptide photoswitching.

XAFS Characterization of NP Photoswitching

To investigate the peptide reconfiguration event due to the photoswitch isomerization, three samples were measured by XAFS before and after UV light exposure: AuBP1C-MAM-, MAM-CAuBP1-, and AuBP1-capped Au NPs. The last sample was prepared in an identical manner, but it used the parent AuBP1 peptide without a photoswitch in the sequence where this sample is termed Au control. The normalized Au L_3-edge XANES spectra of the samples as well as the Au foil spectrum are shown in Figure S1 and S2. The Au control, AuBP1C-MAM- and MAM-CAuBP1-capped NPs exhibit lower fine structure intensities in the main absorption edge area compared to the Au foil due to the NP size effect,[20] as shown in greater detail in Figure S2. The changes in the white line region of NPs passivated by MAM-CAuBP1 before and after UV light exposure (Figure S2) correlate with the ligand reconfiguration due to the photoswitch isomerizing. Prior studies have reported similar intensity changes, consistent with the observed variations in the interaction between the Au NPs and their surrounding ligands.[20]

The EXAFS data in *k*-space and *r*-space are shown in Figure 2. The decrease of the amplitude (in 2~3.5 Å region) of EXAFS spectra for the samples in Figure 2 d-e compared to the bulk Au foil spectrum is caused by the NP size effect.[21] Consistent with the effect of the UV light, and the subsequent change in the interaction between the Au NPs and the

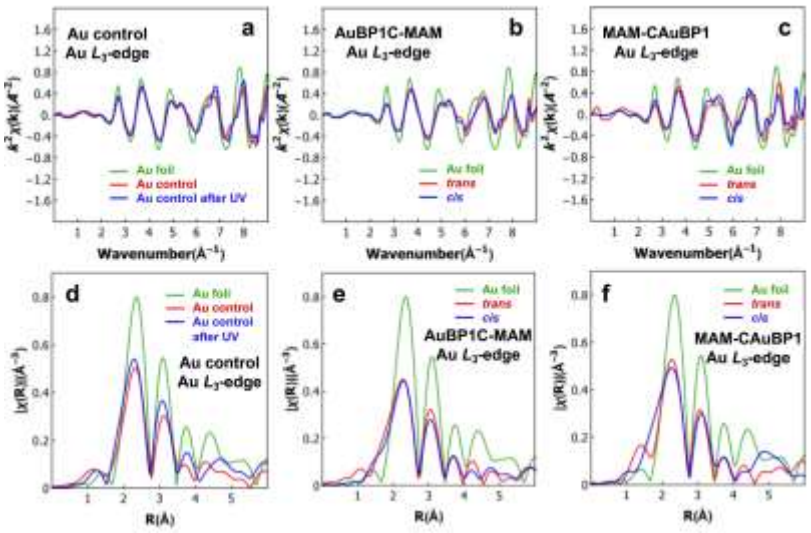

Figure 2. EXAFS *k*-space (parts (a-c)) and *r*-space (parts (d-f)) analysis of the (a and d) Au control, (b and e) AuBP1C-MAM-capped Au NPs, and (c and f) MAM-CAuBP1-capped Au NPs.

peptides, the peak intensity (1.5~2 Å region) in Figure 2e for the AuBP1C-MAM-capped Au NPs increased for the samples measured after the UV light exposure. However, for the MAM-CAuBP1-capped materials in the same *r*-range, the trend is reversed. Such effects can be correlated with the photoswitch *trans* to *cis* induced change in orientation of the peptides and the subsequent change in the Au-X interaction (X =N or C) between Au and the biomolecules. To quantitatively detect the information about the Au - ligand interaction, and its sensitivity to peptide isomerization, the EXAFS data was analyzed by a non-linear multiple least squared method, as implemented in the Artemis package.[22] The experimental EXAFS data fit the theoretical contributions that included the Au-Au and Au-N first nearest neighboring paths. The best fit value of the amplitude reduction factor was obtained to be 0.85, from the analysis of the Au foil EXAFS data (Figure S3). It was subsequently fixed to that value in the fits of the NP samples.

To include the Au-X interaction between the peptide and Au NPs, the crystallographic structure of AuN[23] was used for calculating Au-X (X is a general symbol for a nearest neighboring ligand to Au that can be N or C) nearest neighboring photoelectron scattering amplitude and phase shift using FEFF6.2.[22] Due to the limited *k* range in the data caused by the low concentration of Au in solution (~0.2 mM), the analysis of all samples was done by using multiple data set fitting and by applying several constraints as described below. Because the focus was on the change in the peptide confirmation that was expected to affect primarily the Au-X coordination number (CN), the bond length disorder parameters (σ^2), which correlated with the CNs in the fits, were constrained to vary as the same global parameters for all the samples. To improve the sensitivity to the interatomic distances, the correction to the photoelectron energy origin (ΔE_0) was constrained to be the same global variable as well. That approximation was justified by the alignment of all the data in energy (Figure S1). Finally, the CN(Au-Au) was approximated to be

the same before and after UV light exposure in each sample, so that would focus on the Au-X CN changes due to the UV exposure; the Au-Au CN was not expected to be affected by UV light.

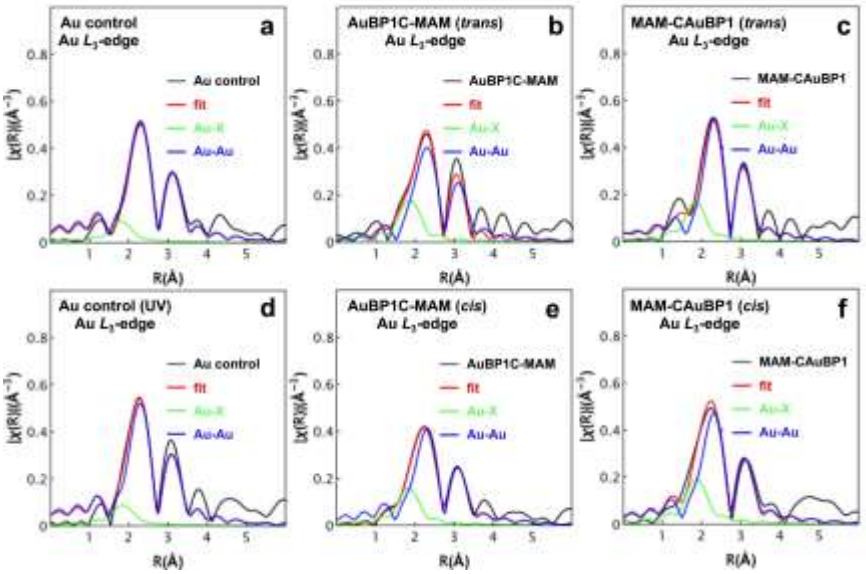

Figure 3. EXAFS fitting results, including both the Au-Au and Au-X fitting paths, for the Au NPs capped with the (a and d) parent AuBP1, (b and e) AuBP1C-MAM, and (c and f) MAM-CAuBP1 peptides. Parts (a-c) present the analysis before UV light exposure (*i.e. trans*), while parts (d-f) display the samples after UV light exposure (*i.e. cis*).

Table 1. Comparison of EXAFS determined CN values, bond lengths, and σ^2 parameters.

Sample	N(Au-Au)	R(Au-Au), Å	σ^2 (Au-Au), Å^2	N(Au-X)	R(Au-X), Å	σ^2 (Au-X), Å^2
Au Control	8.9 ± 0.8	2.839 ± 0.009	0.010 ± 0.001	0.56 ± 0.30	2.493 ± 0.054	0.000 ± 0.008
Au Control (UV)	8.9 ± 0.8	2.831 ± 0.012	0.010 ± 0.001	0.59 ± 0.45	2.495 ± 0.075	0.000 ± 0.008
AuBP1C-MAM (*trans*)	7.2 ± 0.7	2.833 ± 0.017	0.010 ± 0.001	1.07 ± 0.69	2.535 ± 0.055	0.000 ± 0.008
AuBP1C-MAM (*cis*)	7.2 ± 0.7	2.843 ± 0.015	0.010 ± 0.001	0.90 ± 0.52	2.466 ± 0.056	0.000 ± 0.008
MAM-CAuBP1 (*trans*)	8.2 ± 1.0	2.843 ± 0.013	0.010 ± 0.001	0.94 ± 0.67	2.527 ± 0.056	0.000 ± 0.008
MAM-CAuBP1 (*cis*)	8.2 ± 1.0	2.838 ± 0.018	0.010 ± 0.001	1.21 ± 0.83	2.480 ± 0.058	0.000 ± 0.008

The Fourier transform parameters are described in the Supporting Information, Table S1, and the fitting results are summarized in Figure 3 and Table 1. Both of the Au-Au and Au-X fitting paths are shown in Figure 3, where the effect of Au-X is clearly captured in the 1.5~2 Å range. In this analysis, the AuBP1C-MAM- and MAM-CAuBP1-passivated Au NPs, before and after UV light exposure, show a higher peak amplitude in the Au-X fitting path and larger Au-X CN values compared to Au control samples. This likely arises from the azobenzene moiety in the photoswitchable biomolecules that gives rise to a higher Au-X coordination. When comparing the effect of photoswitch isomerization for the AuBP1C-MAM-capped Au NPs (Table 1), the sample presents a Au-X CN value of 1.1 in the

trans configuration; however, after UV exposure the system demonstrated a decreased value of 0.9 for the peptides in the *cis* conformation. Interestingly, for the MAM-CAuBP1-capped materials, an opposite Au-X CN trend was observed wherein the particles in the *cis* conformation had a higher value compared to the *trans* (0.9 for *trans vs*. 1.2 for *cis*). The uncertainties in the mean values were significant (0.5 to 0.8, depending on the sample) and these results are being discussed later in terms of their correlation with the corresponding changes in the reactivity. Furthermore, both of the Au NPs passivated by AuBP1C-MAM and MAM-CAuBP1 show shorter bond length of Au-X after the UV illumination, but the AuBP1C-MAM-based system exhibited a larger decrease of the Au-X bond length (-0.07 Å) compared to the MAM-CAuBP1 with a decrease of 0.05 Å. Such changes are substantially different as compared to the Au control (*e.g.* the Au NPs capped with the AuBP1 peptide without a photoswitch) where negligible differences in the Au-X CN and bond length are observed before and after UV light exposure. These differences are consistent with the hypothesis that altered biomolecular surfaces are present on the Au NPs for the photoswitch-based peptides in the two different isomerization states. To further test this hypothesis, the changes in the catalytic activity were investigated, as described below. Indeed, the claim of the differences in surface structure, indicated but not uniquely proven by EXAFS analysis alone, will be strengthened if their correlation with the corresponding changes in catalytic activity is observed.

Catalytic Analysis

After confirmation of NP production and peptide photoswitching spectroscopically, the catalytic activity of the materials in both the *trans* and *cis* conformations were studied for nitrophenol reduction reactions. For this, a variety of nitro-substituted phenols were examined beyond the

traditional 4-nitrophenol system, including substrates that varied the position of the nitro group (2-nitrophenol (2-NP), 3-nitrophenol (3-NP), and 4-nitrophenol (4-NP)), as well as reactants with two nitro groups (2,3-dinitrophenol (2,3-DNP), 2,4-dinitrophenol (2,4-DNP), and 3,4-dinitrophenol (3,4-DNP)). For this reaction the substrates were reduced to their aminophenol equivalents directly on the metallic surface where differences in the exposed active sites (*trans vs. cis*), in addition to the positions of the nitro group on the substrates, could result in catalytic activity changes. The reactions were monitored using UV-vis where excess $NaBH_4$ was used to catalytically reduce the nitrophenols (Scheme 2). In this case, the reaction is *pseudo* first order with respect to the substrate, consistent with prior studies,[24, 25] where consumption of the substrate was used to measure the rate constant (k_{obs}). Note that for the disubstituted substrates, the k_{obs} values for only the first step of the reduction process was measured.

Scheme 2. Model reactions for the reduction of (a) mono and (b) disubstituted nitrophenols to their respective aminophenol products.

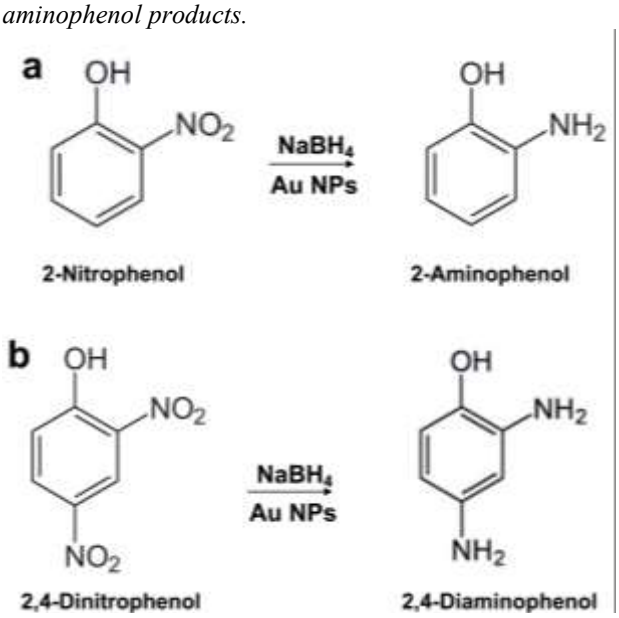

Figure 4 shows the catalytic reactivity analysis for the Au NPs capped with AuBP1C-MAM in the *trans* state using 2-NP and 2,4-DNP as the substrates. Figure 4a specifically displays the decrease in absorbance at 411 nm arising from the consumption of 2-NP during the reduction reaction to generate 4-aminophenol. Plotting this change in absorbance over time (Figure 4b) demonstrates that the reaction quickly reached completion within 200 s. Visual analysis of the reaction showed that the color of the system changed from bright yellow for the nitro containing compound to clear for the aminophenol-based product, consistent with prior studies of similar

reactions.[26, 27] To calculate the reaction rate constant, a plot of ln (A/A_o) versus time was plotted, where A and A_0 represent the absorbance at time t and 0 s, respectively. From this plot, the slope of the best fit line over the linear region can be used to calculate the rate constant. Plotting of this analysis for the 2-NP reaction, as shown in Figure 4c, resulted in a k_{obs} of (5.4 ± 1.5) × 10^{-3} s^{-1}.

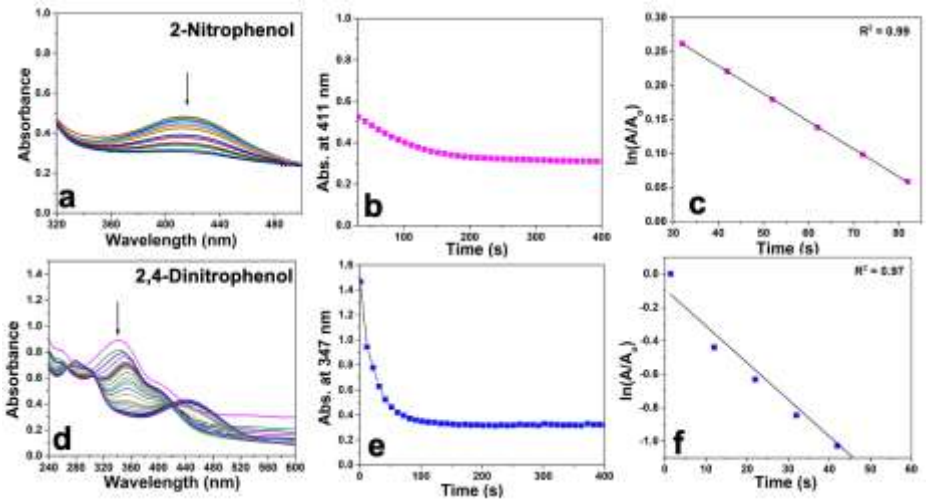

Figure 4. Catalytic analysis for the reduction of (a-c) 2-nitrophenol and (d-f) 2,4-dinitrophenol using the AuBP1C-MAM-capped Au NPs in the *trans* configuration. Parts (a and d) present the UV-vis spectra, parts (b and e) show the absorbance intensity plot for the substrate as a function of time, while parts (c and f) display the ln(A/A_0) plots over time from which k_{obs} values can be determined.

The exact same process was employed for the reaction using the AuBP1C-MAM capped Au NPs with the biomolecules in the *cis* configuration. For this, the materials were irradiated with UV light for 30 min prior to reaction analysis. Once the photostationary state was reached, the reaction was initiated. It is important to note that the half-life of the molecule on the Au NP surface is 321 ± 22 h,[14] which is substantially longer than the reaction time. From this system, a k_{obs} value of (3.6 ± 1.1) × 10^{-3} s^{-1} was observed (Figure 5a), which is lower than the value for the same materials with the peptides in the *trans* conformation.

Identical approaches were used for the catalytic reduction analysis using the AuBP1C-MAM-capped Au NPs in both the *trans* and *cis* configurations using the different single substituted nitrophenol compounds (3-NP and 4-NP – Figure 5a). Remarkably enhanced reactivity was noted using 3-NP where rate constants of (147.8 ± 15.0) × 10^{-3} and (111.9 ± 13.0) × 10^{-3} s^{-1} were observed

with the peptides in the *trans* and *cis* conformation, respectively. For the final single nitro group compound, 4-NP, slower reactivity was noted with k_{obs} values of (24.4 ± 15.3) × 10^{-3} s^{-1} for the *trans* configuration and (2.53 ± 1.0) × 10^{-3} s^{-1} for the *cis* AuBP1C-MAM-based Au NPs.

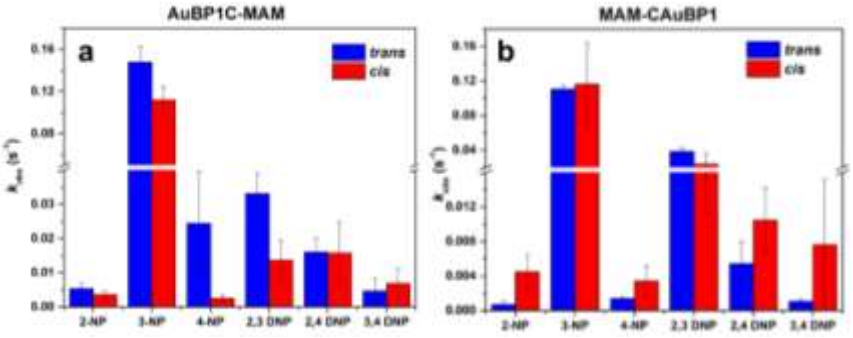

Figure 5. Comparison of k_{obs} values quantified for the indicated substrates using the (a) AuBP1C-MAM and (b) MAM-CAuBP1 peptides in the *trans* and *cis* configurations.

The reaction analysis was further advanced to new substrates with two nitro groups in the phenol structure. To minimize the complexity of the reaction, k_{obs} values for just the reduction of the first nitro substituent is reported. Figure 4d presents the kinetic UV-vis analysis for the reduction for 2,4-DNP. The UV-vis spectra are quite complex; however, the decrease in the substrate absorbance at 347 nm was used to monitor the initial reduction process, which was completed within 200 s (Figure 4e). Calculation of the rate constant from the plot of Figure 4f was used, giving rise to a k_{obs} value of (16.0 ± 4.1) × 10^{-3} s^{-1} for the AuBP1C-MAM-capped Au NPs in the *trans* configuration. When the same process was driven by the NPs in the *cis* conformation, a slightly diminished rate constant of (15.7 ± 9.0) × 10^{-3} s^{-1} was determined (Figure 5a). Similar reaction results were observed for the two additional di-substituted nitrophenol substrates (2,3-DNP and 3,4-DNP). To this end, when 2,3-DNP was employed as the substrate for the reaction catalyzed by the AuBP1C-capped Au NPs in the *trans* and *cis* configurations, k_{obs} values of (33.1 ± 6.0) × 10^{-3} s^{-1} and (13.7 ± 6.0) × 10^{-3} s^{-1} were calculated, respectively; however, for the 3,4-DNP substrate, diminished rate constants of (4.7 ± 3.5) × 10^{-3} s^{-1} for the *trans* materials and (6.9 ± 4.2) × 10^{-3} s^{-1} for the *cis*-based system were determined.

The same set of reduction reactions was carried out using MAM-CAuBP1 capped Au NPs (Figure 5b). For this system in the *trans* conformation, the k_{obs} values for the reduction of 2-NP, 3-NP, and 4-NP was $(0.7 \pm 0.4) \times 10^{-3}$, $(110.5 \pm 4.5) \times 10^{-3}$, and $(1.4 \pm 0.2) \times 10^{-3}$ s^{-1}, respectively. When the reaction was processed using the di-substituted substrates with the *trans*-based material, rate constants of $(38.4 \pm 4.6) \times 10^{-3}$ s^{-1} for 2,3-DNP, $(5.4 \pm 2.6) \times 10^{-3}$ s^{-1} for 2,4-DNP, and $(1.1 \pm 0.2) \times 10^{-3}$ $s^{-1}$for 3,4-DNP were observed. Switching of the peptides conformation to the *cis* form for the MAM-CAuBP1-capped Au NPs resulted in changes to the observed rate constants. To this end, when the reaction was processed with 2-NP, a k_{obs} value of $(4.5 \pm 2.0) \times 10^{-3}$ s^{-1} was noted, which is significantly greater than for the same materials with the peptide in the *trans* configuration. For the 3-NP and 4-NP substrates, rate constants of $(116.2 \pm 47.6) \times 10^{-3}$ s^{-1} and $(3.4 \pm 1.7) \times 10^{-3}$ s^{-1} were noted, respectively, for the *cis*-based materials. Finally, for the disubstituted substrates, 2,3-DNP, 2,4-DNP, and 3,4-DNP, k_{obs} values of $(23.9 \pm 2.8) \times 10^{-3}$ s^{-1}, $(10.4 \pm 3.7) \times 10^{-3}$ s^{-1}, and $(7.6 \pm 7.6) \times 10^{-3}$ s^{-1} were determined, respectively (Figure 5b).

When comparing the reactivity between the mono-substituted nitrophenols, 3-NP exhibited the highest catalytic reactivity by a significant degree. In general, the reactivity of nitrophenols depends on the formation of the nitrophenolate ion and its stability, where the stability of this ion follows an order of 4-NP > 2-NP > 3-NP.[28] For the 4-nitrophenolate ion, conjugation within the ring structure leads to this enhanced stability, where the negative charge on the oxygen is delocalized through the benzene ring. For the 2-nitrophenolate ion of intermediate stability, conjugation with the ring plays an effect, but due to steric hinderance of the neighboring hydroxyl group, it is less stable than 4-NP. When considering the 3-nitrophenolate ion, this species has an inductive effect from the nitro group but not a conjugative effect, thus making it the least stable

species. As a result, higher catalytic reactivity for 3-NP is anticipated, which was observed in the present study.

Based on the stability of the monofunctionalized substrates, the anticipated stability of the bifunctionalized nitrophenolate species would follow an order of 2,4-DNP > 3,4-DNP > 2,3-DNP. In general, 2,3-DNP is the least stable among the three as the nitro groups are in the *meta* and *ortho* position, having no conjugative effect (*meta* position), coupled with steric hinderance (*ortho* position). Together, this makes the 2,3-dinitrophenolate ion more unstable as compared with the other dinitrophenolate ions. This effect was observed in the catalytic reactivity of the dinitrophenols, where 2,3-DNP exhibited the highest reactivity compared to 2,4-DNP and 3,4-DNP for MAM-CAuBP1 in both the *trans* and *cis* conformations.

Considering the reactivity trend between both peptides (AuBP1C-MAM and MAM-CAuBP1), and the two conformations (*trans* vs *cis*), some differences were observed across all nitrophenol reductions. With the Au NPs capped with AuBP1C-MAM peptide (Figure 5a), higher k_{obs} values were generally observed with the NPs in the *trans* configuration over the *cis*, especially when considering the monosubstituted nitrophenols. This suggests that optimal metallic or active site exposure for reactivity was accessed in the *trans* configuration; however, the molecular structure of the substrate plays a role in this effect. For instance, higher reactivity was noted for 3,4-DNP in the *cis* configuration of the AuBP1C-MAM peptide as compared to the *trans* system. Such effects may arise from the positioning of the two nitro groups with respect to the alcohol functionality; however, additional studies are required to more fully explore this effect.

When considering the NPs with the MAM-CAuBP1 capping system, an opposite trend of greater reactivity with the *cis*-based peptide was observed in general. While not all of the substrate demonstrated this effect, further suggesting molecular structural effects, the majority of systems

did present greater k_{obs} values for the *cis* peptide conformation. Taken together, this suggests that the NP system is sensitive to the photoswitch position in the peptide, which likely affects both the structural change ability, as well as the bio-overlayer configuration in the two different conformations. This, in turn, could have significant impacts on the catalytic functionality.

An interesting correlation between the observed catalytic reactivity of the materials and the spectroscopic results is also evident. For the materials with the peptide in the more reactive configuration (*trans* for AuBP1C-MAM and *cis* of MAM-CAuBP1), a higher Au-X CN value is noted from the XAFS studies. This suggests that a strong Au-X coordination may be required to enhance the reaction, which may arise from changes in the electronic environment at the NP surface to facilitate the interaction between the nitrophenol-based substrate and the NP metallic surface. Further studies are required to monitor the reaction *in situ* to probe this effect; however, this correlation between the spectroscopic results and the reactivity strongly suggests that changes in the bioligand overlayer structure are important in modulating the reactivity.

When comparing the reactivity of the present study to previous work, several publications have reported the reduction of 2-NP, 3-NP, and 4-NP using supported metal NPs. Xia *et al.* synthesized a carbon black supported nickel NP for the reduction of the three monosubstituted substrates. In this study, 3-NP and 4-NP exhibited the highest conversion to their anticipated products within 15 min, however a different metallic composition was used for the reaction[29] Sun *et al.* examined the hydrogenation of 2-NP, 3-NP, 4NP, and 2,4-DNP using a stable palladium/graphene nanocomposite. Due to conjugation, induction, and steric effects, the reactivity of nitrophenols observed were 3-NP > 2-NP > 4-NP > 2,4-DNP.[30] Similar trends were noted here, especially when considering the monosubstituted nitrophenols, but again, a different material metallic composition was employed for this work. Gerelbaatar *et al.* studied the reduction of 2,4-dinitrophenol to 2,4-

diaminophenol using Au and Ag NPs. Complete reduction to 2,4-diaminophenol was observed in 72 min with Au NPs, and in 108 min with Ag NPs.[17] Taken together, enhanced reactivity was generally observed from the peptide-capped materials; however, the ability to modulate the reactivity via external stimuli presents opportunities to control the process at unique and new levels.

CONCLUSIONS

In conclusion, these studies provide direct spectroscopic correlations between changes in peptide ligand overlayer structures achieved via remote stimuli and catalytic reactivity differences from the materials in the different bioligand configurations. The reactivity was demonstrated to be significantly affected by the position of the photoswitch within the peptide structure, as well as the substrate selected for the reaction. To this end, changes in the nitro group position and number played important roles in controlling the reactivity. Remarkably, direct correlations between the catalytic reactivity and the ligand surface coordination changes as a function of isomerization were observed, suggesting that changes in the ligand overlayer structure are indeed the basis of the variations in the reactivity. Such studies support the ability to exploit remote stimuli to modulate NP catalytic functionality, which could be important to achieve controlled catalytic processes via NP-based materials that remains challenging to achieve. Such capabilities could also impact a variety of other nanomaterial-based applications from drug delivery to sensing, making the ability to remotely stimulate or actuate NP-bound ligand interfaces an interesting target to control functionality.

Supporting Information. XANES Spectra, Fourier transform parameters, and fitting results. The Supporting Information is available free of charge on the ACS Publications website at DOI: XXX.

Acknowledgement. This work was supported by the National Science Foundation under grant 1903649 (MRK) and 1903576 (AIF). This research used beamline 8-ID of the National Synchrotron Light Source II, a U.S. Department of Energy (DOE) Office of Science User Facility operated for the DOE Office of Science by Brookhaven National Laboratory under Contract No. DE-SC0012704.

REFERENCES

1. Wang, L.; Xu, L.; Kuang, H.; Xu, C.; Kotov, N. A., Dynamic nanoparticle assemblies. *Acc. Chem. Res.* **2012,** *45*, 1916-1926.

2. Lüning, U., Switchable Catalysis. *Angew. Chem. Int. Ed.* **2012,** *51*, 8163-8165.

3. Tang, Z.; Lim, C.-K.; Palafox-Hernandez, J. P.; Drew, K. L. M.; Li, Y.; Swihart, M. T.; Prasad, P. N.; Walsh, T. R.; Knecht, M. R., Triggering nanoparticle surface ligand rearrangement via external stimuli: light-based actuation of biointerfaces. *Nanoscale* **2015,** *7*, 13638-13645.

4. Stoll, R. S.; Hecht, S., Artificial Light-Gated Catalyst Systems. *Angew. Chem. Int. Ed.* **2010,** *49*, 5054-5075.

5. Lawrence, R. L.; Cendan, V. J.; Scola, B.; Liu, Y.; Lim, C.-K.; Prasad, P. N.; Swihart, M. T.; Knecht, M. R., Optical Control of Biomimetic Nanoparticle Catalysts Based upon the Metal Component. *J. Phys. Chem. C* **2018,** *122*, 28055-28064.

6. Chaturvedi, S.; Dave, P. N.; Shah, N. K., Applications of nano-catalyst in new era. *J. Saudi Chem. Soc.* **2012,** *16*, 307-325.

7. Briggs, B. D.; Knecht, M. R., Nanotechnology Meets Biology: Peptide-based Methods for the Fabrication of Functional Materials. *J. Phys. Chem. Lett.* **2012,** *3*, 405-418.

8. Besson, M.; Gallezot, P.; Pinel, C., Conversion of Biomass into Chemicals over Metal Catalysts. *Chem. Rev.* **2014,** *114*, 1827-1870.

9. Munnik, P.; de Jongh, P. E.; de Jong, K. P., Recent Developments in the Synthesis of Supported Catalysts. *Chem. Rev.* **2015,** *115*, 6687-6718.

10. Tang, Z.; Palafox-Hernandez, J. P.; Law, W.-C.; Hughes, Z. E.; Swihart, M. T.; Prasad, P. N.; Knecht, M. R.; Walsh, T. R., Biomolecular Recognition Principles for

Bionanocombinatorics: An Integrated Approach To Elucidate Enthalpic and Entropic Factors. *ACS Nano* **2013,** *7*, 9632-9646.

11. Neilson, B. M.; Bielawski, C. W., Illuminating Photoswitchable Catalysis. *ACS Catal.* **2013,** *3*, 1874-1885.

12. Lawrence, R. L.; Hughes, Z. E.; Cendan, V. J.; Liu, Y.; Lim, C.-K.; Prasad, P. N.; Swihart, M. T.; Walsh, T. R.; Knecht, M. R., Optical Control of Nanoparticle Catalysis Influenced by Photoswitch Positioning in Hybrid Peptide Capping Ligands. *ACS Appl. Mater. Interfaces* **2018,** *10*, 33640-33651.

13. Lawrence, R. L.; Scola, B.; Li, Y.; Lim, C.-K.; Liu, Y.; Prasad, P. N.; Swihart, M. T.; Knecht, M. R., Remote Optically Controlled Modulation of Catalytic Properties of Nanoparticles through Reconfiguration of the Inorganic/Organic Interface. *ACS Nano* **2016,** *10*, 9470-9477.

14. Lawrence, R. L.; Olagunju, M. O.; Liu, Y.; Mahalingam, K.; Slocik, J. M.; Naik, R. R.; Frenkel, A. I.; Knecht, M. R., Remote controlled optical manipulation of bimetallic nanoparticle catalysts using peptides. *Catal. Sci.Techol.* **2021,** *11*, 2386-2395.

15. Gerelbaatar, K.; Tsogoo, A.; Dashzeveg, R.; Tsedev, N.; Ganbold, E. O., Reduction of 2,4-Dinitrophenol to 2,4-Diaminophenol Using AuNPs and AgNPs as Catalyst. *Solid State Phenom.* **2018,** *271*, 76-84.

16. Li, Y.; Tang, Z.; Prasad, P. N.; Knecht, M. R.; Swihart, M. T., Peptide-mediated synthesis of gold nanoparticles: effects of peptide sequence and nature of binding on physicochemical properties. *Nanoscale* **2014,** *6*, 3165-3172.

17. Creighton, J. A.; Eadon, D. G., Ultraviolet–visible absorption spectra of the colloidal metallic elements. *J. Chem. Soc. Faraday Trans.* **1991,** *87*, 3881-3891.

18. Behafarid, F.; Matos, J.; Hong, S.; Zhang, L.; Rahman, T. S.; Roldan Cuenya, B., Structural and electronic properties of micellar Au nanoparticles: size and ligand effects. *ACS Nano* **2014,** *8*, 6671-6681.

19. Frenkel, A. I.; Hills, C. W.; Nuzzo, R. G., A View from the Inside: Complexity in the Atomic Scale Ordering of Supported Metal Nanoparticles. *J. Phys. Chem. B* **2001,** *105*, 12689-12703.

20. Newville, M., IFEFFIT : interactive XAFS analysis and FEFF fitting. *J. Synchrotron Radiat.* **2001,** *8*, 322-324.

21. Chen, W.; Jiang, J. Z., Elastic properties and electronic structures of 4d- and 5d-transition metal mononitrides. *J. Alloys Compd.* **2010,** *499*, 243-254.

22. Neal, R. D.; Inoue, Y.; Hughes, R. A.; Neretina, S., Catalytic Reduction of 4-Nitrophenol by Gold Catalysts: The Influence of Borohydride Concentration on the Induction Time. *J. Phys. Chem. C* **2019,** *123*, 12894-12901.

23. Ai, L.; Jiang, J., Catalytic reduction of 4-nitrophenol by silver nanoparticles stabilized on environmentally benign macroscopic biopolymer hydrogel. *Bioresour. Technol.* **2013,** *132*, 374-377.

24. Ma, M.; Yang, Y.; Li, W.; Feng, R.; Li, Z.; Lyu, P.; Ma, Y., Gold nanoparticles supported by amino groups on the surface of magnetite microspheres for the catalytic reduction of 4-nitrophenol. *J. Mater. Sci.* **2019,** *54*, 323-334.

25. Feng, Y.; Yin, J.; Liu, S.; Wang, Y.; Li, B.; Jiao, T., Facile Synthesis of Ag/Pd Nanoparticle-Loaded Poly(ethylene imine) Composite Hydrogels with Highly Efficient Catalytic Reduction of 4-Nitrophenol. *ACS Omega* **2020,** *5*, 3725-3733.

26. Jana, S.; Ghosh, S. K.; Nath, S.; Pande, S.; Praharaj, S.; Panigrahi, S.; Basu, S.; Endo, T.; Pal, T., Synthesis of silver nanoshell-coated cationic polystyrene beads: A solid phase catalyst for the reduction of 4-nitrophenol. *Appl. Catal. A - Gen.* **2006,** *313*, 41-48.

27. Xia, J.; He, G.; Zhang, L.; Sun, X.; Wang, X., Hydrogenation of nitrophenols catalyzed by carbon black-supported nickel nanoparticles under mild conditions. *Appl. Catal. B - Environ.* **2016,** *180*, 408-415.

28. Sun, J.; Fu, Y.; He, G.; Sun, X.; Wang, X., Catalytic hydrogenation of nitrophenols and nitrotoluenes over a palladium/graphene nanocomposite. *Catal. Sci. Technol.* **2014,** *4*, 1742-1748.

FOR TABLE OF CONTENTS USE ONLY